applied sciences

MDPI

Article

Compact 6 dB Two-Color Continuous Variable Entangled Source Based on a Single Ring Optical Resonator

Ning Wang [1,2], Shanna Du [1,2] and Yongmin Li [1,2,*]

[1] State Key Laboratory of Quantum Optics and Quantum Optics Devices, Institute of Opto-Electronics, Shanxi University, Taiyuan 030006, China; lylawang@foxmail.com (N.W.); dushanna93@163.com (S.D.)
[2] Collaborative Innovation Centre of Extreme Optics, Shanxi University, Taiyuan 030006, China
* Correspondence: yongmin@sxu.edu.cn; Tel.:+86-351-7011-575

Received: 26 January 2018; Accepted: 24 February 2018; Published: 26 February 2018

Abstract: Continuous-variable entangled optical beams at the degenerate wavelength of 0.8 μm or 1.5 μm have been investigated extensively, but separately. The two-color entangled states of these two useful wavelengths, with sufficiently high degrees of entanglement, still lag behind. In this work, we analyze the various limiting factors that affect the entanglement degree. On the basis of this, we successfully achieve 6 dB of two-color quadrature entangled light beams by improving the escape efficiency of the nondegenerate optical amplifier, the stability of the phase-locking servo system, and the detection efficiency. Our entangled source is constructed only from a single ring optical resonator, and thus is highly compact, which is suitable for applications in long-distance quantum communication networks.

Keywords: quantum optics; continuous variable entangled states; nondegenerate optical parametric amplifier

1. Introduction

Squeezed states and quantum entanglement [1] are essential resources for constructing quantum information networks, performing ultrasensitive quantum measurements, and implementing speedy quantum computing [2–9]. For instance, squeezed (entangled) states are necessary in order to improve the sensitivities of spectroscopic measurement [10,11], velocimetry [12], light detection and ranging equipment [13], gravitational wave detection [7,8], and quantum key distribution [14,15]. For future quantum networks, the quantum repeater protocol is indispensable for implementing the distribution of quantum-entangled states over long distances via quantum memory and entanglement swapping [16–18]. To this end, one desires a compact entangled source with a high degree of entanglement at the non-degenerate frequencies of 0.8 μm and 1.5 μm. The 0.8 μm wavelength is compatible with the quantum memory device, which consists of alkaline atoms, and the 1.5 μm wavelength is compatible with telecommunication optical fibers. In addition, such entangled sources are valuable to long-distance continuous variable (CV) quantum key distribution, allowing one to significantly extend the distribution distance and tolerate excess noise, as shown by Madsen et al. in Ref. [14].

Non-degenerate optical parametric amplifiers (NOPAs) are powerful tools for preparing high quality CV quantum-entangled light fields. Various entangled states, including two-color [19–25] and three-color [26–28] CV quantum-entangled states, have been generated. We have utilized a single ring resonator, which combines both the NOPA and non-degenerate optical parametric oscillator (NOPO), and prepared quantum-entangled states with a large wavelength difference. In previous

works, the generated two-color CV quantum-entangled states only produced 3.3 dB of quadrature squeezing [6], which is less attractive for quantum information processing, where a high degree of entanglement is desired. In this paper, we analyze the relevant factors, such as the total efficiency of the optical system and the fluctuation of the phase-locking, which are crucial to the degree of entanglement. Based on simulation results, we improved and optimized the experimental system and successfully increased the two-color CV entanglement from 3.3 dB to 6 dB, which is the best result using this design, to our knowledge.

2. Theoretical Analysis

In order to improve the entanglement preparation system, we first analyze the factors that are crucial to the entanglement quality. For a NOPA, the measurable level of the quantum noise spectrum of the amplitude quadrature difference (phase quadrature sum) can be modeled by [29,30]:

$$V_{sq(Anti-sq)} = 1 + 4\sqrt{P/P_{th}}\eta_{\mathrm{tot}}[\frac{\sin^2(\theta+\alpha_{\pm})}{(1-\sqrt{P/P_{th}})^2+4(f/f_c)^2} - \frac{\mathrm{COS}^2(\theta+\alpha_{\pm})}{(1+\sqrt{P/P_{th}})^2+4(f/f_c)^2}] \quad (1)$$

where $\alpha_{\pm}=0$ and $\alpha_{\pm}=\pi/2$ correspond to the squeezing spectrum and anti-squeezing spectrum, respectively. P and P_{th} are the pump power and the oscillation threshold of the NOPA, respectively, η_{tot} is the total efficiency of the system, f is the analysis frequency, f_c is the decay rate of the optical cavity, and θ is the root mean squared (RMS) phase fluctuation of the locking between the local oscillator (LO) and the signal field. From the above model, we find that the entanglement quality depends on four factors: the pump power level of the NOPA (P/P_{th}), the total efficiency of the system (η_{tot}), the normalized analysis frequency f/f_c, and the fluctuation of the phase locking (θ).

The total efficiency of the system consists of five parts: $\eta_{\mathrm{tot}} = \eta_{\mathrm{esc}} \times \eta_{\mathrm{t}} \times \eta_{\mathrm{vis}} \times \eta_{\mathrm{pd}} \times \eta_{\mathrm{en}}$. The quantity η_{esc} is the escape efficiency of the NOPA cavity, defined as $\eta_{\mathrm{esc}} = \frac{T}{T+L}$ and L present the amplitude transmittance of the output coupling mirror, and the intracavity round trip loss, respectively. The quantity η_{t} is the propagation efficiency, and η_{vis} is the interference efficiency with $\eta_{\mathrm{vis}} = v^2$, where v is the interference visibility of the homodyne detection, which is the quality of the spatial mode overlapping between the signal and the LO on the 50/50 beam splitter. The quantity η_{pd} is the quantum efficiency of the photodiodes, and η_{en} is the equivalent measurement efficiency that is induced by electronic noise.

Without taking account the phase fluctuation, Equation (1) can be simplified to:

$$V_{sq} = 1 - \eta_{\mathrm{tot}}\frac{4\sqrt{P/P_{th}}}{(1+\sqrt{P/P_{th}})^2+4(f/f_c)^2} \quad (2)$$

$$V_{Anti-sq} = 1 + \eta_{\mathrm{tot}}\frac{4\sqrt{P/P_{th}}}{(1-\sqrt{P/P_{th}})^2+4(f/f_c)^2} \quad (3)$$

Figure 1 shows the simulated quantum correlation spectrum as a function of the analysis frequencies at different total efficiencies. The higher the loss of the system, the lower the squeezing level one can obtain given a certain analysis frequency. Furthermore, the squeezing level decreases with the increase of the analysis frequency, due to the limitation of the cavity linewidth. The squeezing level reaches −9.2 dB at 1 MHz with 10% total loss, while it reduces to −5 dB at 1 MHz when the loss increases to 30%. There is an approximate 4.2 dB gain for the squeezing when the loss is reduced from 30% to 10%.

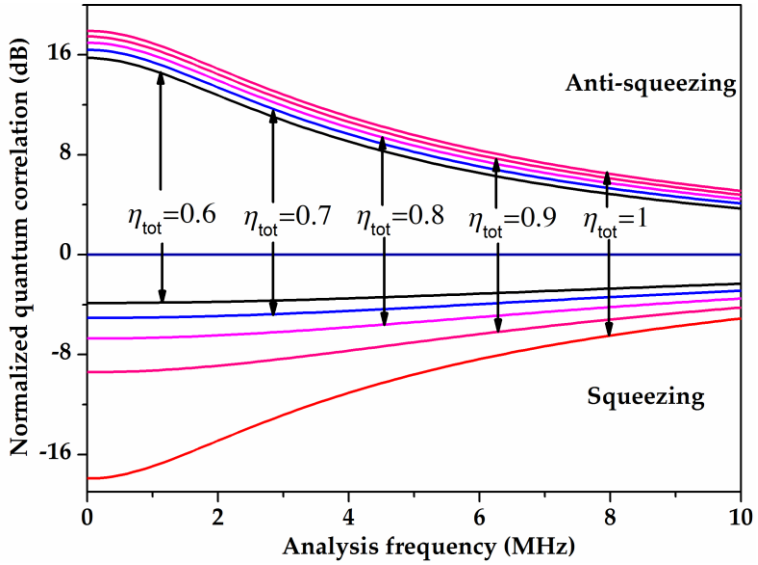

Figure 1. The simulated quantum correlation as a function of the analysis frequency with different total efficiencies. For all curves, $\frac{P}{P_{th}} = 0.6$, $\theta = 0$, and $f_c = 17$ MHz.

The amount of detectable squeezing is not only limited by the optical loss, it is also limited by the fluctuations of the relative phase, which are always present in reality. Considering the phase jitter effects, the realistic squeezing V_{sq} and anti-squeezing $V_{Anti-sq}$ are given by:

$$V_{sq}^{M} = V_{sq}\cos^2\theta + V_{Anti-sq}\sin^2\theta \quad (4)$$

$$V_{Anti-sq}^{M} = V_{sq}\sin^2\theta + V_{Anti-sq}\cos^2\theta \quad (5)$$

Equation (4) indicates that the phase fluctuations inevitably transfer the anti-squeezing noise to the squeezing noise. Figure 2 shows that the phase fluctuations deteriorate the level of measured quantum squeezing, and the squeezing disappears when θ grows to ~7.5 degrees.

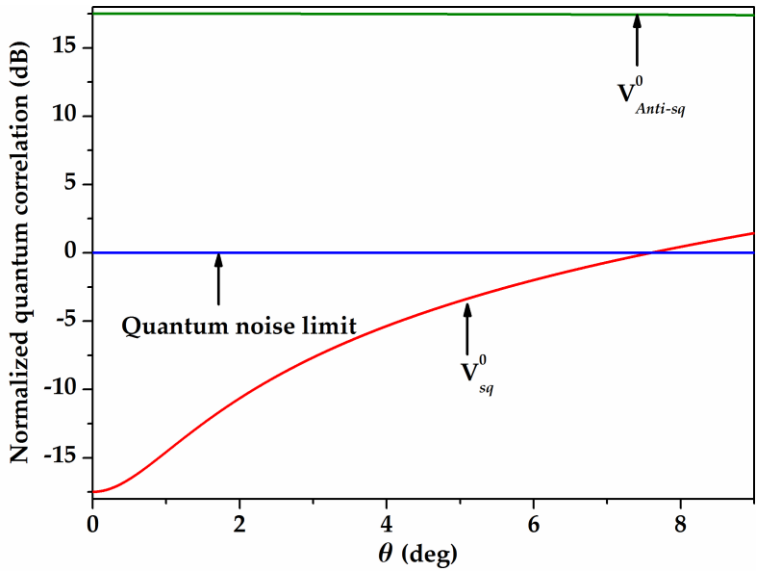

Figure 2. The simulated quantum correlation as a function of the relative phase fluctuation.

3. Experimental Setup

A schematic of our experimental apparatus is shown in Figure 3. The setup includes three parts: the optical devices for entangled state generation, the servo-locking devices, and the balanced homodyne detection (HD) system.

The optical devices part: A single-frequency continuous-wave laser (Cobolt Lasers, Solna, Sweden) at 532 nm was used to pump a NOPO and NOPA from opposite directions. The NOPO and NOPA shared a bowtie-type ring cavity consisting of two concave mirrors (radius of curvature, 50 mm) and two flat mirrors. One of the flat mirrors was a partial transmittance mirror and worked as the output coupler, while the other had high reflectance (~99.9%) at all three wavelengths (pump, signal, and idler). From previous analysis, although high escape efficiency is beneficial to entanglement, the drawback is that it will boost the threshold of the NOPO. There is a compromise between escape efficiency and threshold pump power. In this case, the output coupler was coated for partial transmission (~10.2%) at 0.8 μm and 1.5 μm, and high reflectivity at 532 nm (99.6%). The two input couplers (concave mirrors) were coated for high reflectivity at 0.8 μm and 1.5 μm (>99.9%), and partial transmission at 532 nm (~44%). Here, the design of the partial transmission at 532 nm for the input couplers helps to decrease the NOPO threshold effectively by about 2.2 times.

A 20-mm long periodically poled KTiOPO4 (PPKTP) crystal (Raicol Crystals Ltd, Rosh Ha'Ayin, Israel) placed between the two concave mirrors served as the second-order nonlinear medium. The crystal was especially anti-reflection coated (<0.1%) at both the signal and the idler wavelength in order to reduce intracavity losses as much as possible. The beam waist size inside the crystal was about 30 μm, to allow for optimal focusing of the Gaussian pump beams. To avoid the residual reflection effects from the crystal's surfaces on the stable operation of the NOPO, a parallelogram PPKTP was used, where both end faces were cut at an angle of two degrees.

Inside the cavity, the two directions of the down-converted beams propagated along exactly the same path, and thus share the same linear and nonlinear losses, phase shift, phase-matched conditions, and so on. Therefore, when the cavity length is stabilized, the forward NOPA and backward NOPO both oscillate on a single signal–idler mode pair with the same frequency.

The servo-locking devices: To enable generation of entanglement, the ring cavity was controlled in resonance using a dither-locking servo-control system. To this end, the leaked light from one of the high reflectance flat mirror of the cavity was detected by a photodetector (PD2) and fed into the servo system. The signal-injected NOPA is phase insensitive, and no relative phase-locking is required between the signal and the pump fields [6]. In order to measure the quantum correlation between the amplitude (phase) quadratures, we needed to precisely lock the relative phase at zero or half π between the signal (idler) mode and the corresponding local oscillator (LO) beam in two sets of HD simultaneously. As shown in Section 2, the fluctuations of the relative phase projected noise from the anti-squeezed combined quadratures into the squeezed combined quadratures. For the phase-locking of the half π relative phase, the direct current (DC) signals from each homodyne detection were used as error signals, which were further processed by proportional-integral-derivative controllers (PID) (Stanford Research Systems Inc., Sunnyvale, CA, USA) and amplified to drive the piezoelectric transducers PZT1 and PZT2. For the phase locking of the zero relative phase, we employed a dither-locking approach. In the phase-locking loop, a low pass filter with a 100 kHz cut-off frequency filtered the high-frequency background noise and improved the signal-to-noise ratio.

Although active servo systems were utilized in our system, the passive stability of the system was a prerequisite for the precise stabilization of the cavity length and the relative phase between the LO and the signal beam. Several efforts were implemented in this direction. We placed the NOPA device on an invar plate, and enclosed it in an acrylic plastic glazing cover, in which several small holes were drilled for the pump and down-converted beams. The nonlinear crystal was placed in an oven, which was precisely temperature-controlled in order to maintain the crystal at a constant phase-matching temperature. In all, the observed fluctuation of the relative phase locking was around 8.7 mrad.

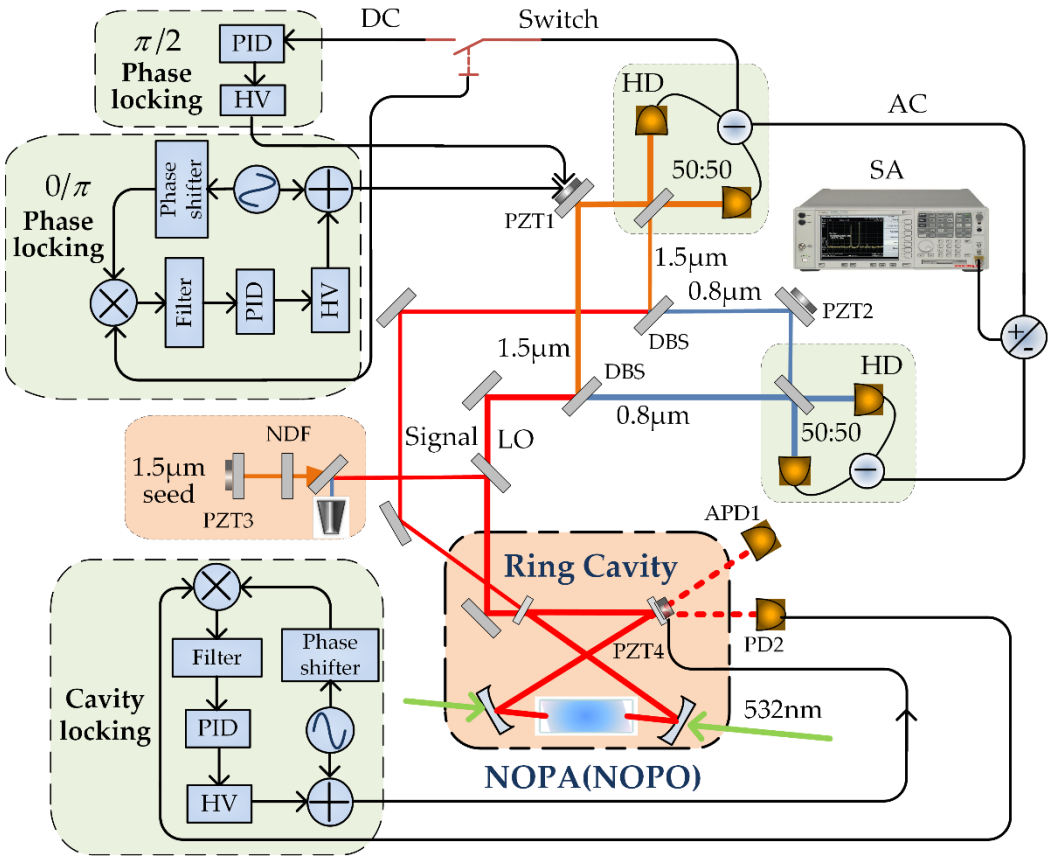

Figure 3. Schematic of the experimental setup. NOPO: nondegenerate optical parametric oscillator; NOPA: nondegenerate optical parametric amplifier; PZT: piezoelectric transducers; PD: photodetectors; APD: avalanche photodetector; HD: balanced homodyne detector, NDF: neutral density filter; LO: local oscillator; DBS: dichroic beam splitter; PID: proportional-integral-derivative controller; HV: high voltage amplifier; SA: spectrum analyzer. Black lines denote the electrical channels for measurement and control. Green line, orange lines, and blue lines represent the pump laser, 1.5 μm, and 0.8 μm optical fields, respectively.

The balanced homodyne detection (HD) system: The quadrature entanglement between the signal and the idler modes were measured with two sets of HD systems. First, the down-converted fields from both the NOPA and NOPO were separated by two dichroic beam splitters (DBS). Then the entangled light fields and the corresponding LO interfered on a 50:50 beam splitter with an interference visibility of 98%, and were subsequently detected by the HDs, which were built from two InGaAs photodiodes (Beijing Lightsensing Technologies Ltd., Beijing, China) and two Si photodiodes (Beijing Hamamatsu Photon Techniques INC, Beijing, China). The measured quantum efficiencies were around 92% at the wavelengths of both 0.8 μm and 1.5 μm. The quantum correlation (anti-correlation) noise spectrum of the amplitude quadrature difference and phase quadrature sum were recorded by a spectrum analyzer.

4. Results and Discussion

The intracavity round trip loss included the residual reflection, absorption, and the scattering from the mirrors and the crystal. Another non-negligible loss of the nonlinear crystal was induced by green light-induced infrared absorption (GLIIRA) [31–33]. In our experiment, we tested two types of nonlinear crystals, MgO: PPLN (Periodically Poled Lithium Niobate) and PPKTP, and compared their GLIIRA effects. Compared with the PPKTP, the MgO: PPLN crystal had a higher nonlinear coefficient; however, the thermal effect due to GLIIRA was more severe, which made the locking of the cavity length very hard. Therefore, we finally chose the PPKTP crystal. Theoretically, the highest entanglement is achieved at the threshold pump power. However, when considering the effect of

GLIIRA, there exists an optimal pump power level for the best entanglement. This is because higher pump power results in a stronger GLIIRA effect, which will spoil the entanglement. In our experiment, the optimal pump power for the NOPO and NOPA are 1.1 times and 0.6 times the threshold power, respectively.

Figure 4 plots the measured quantum correlation between the signal and idler beams at 1.5 μm and 0.8 μm with a spectrum analyzer. The electronic noise of the homodyne detector was 28 dB below the quantum noise limit at 1 MHz, and was not subtracted from the data. The quantum correlation noise of the NOPA output optical fields was recorded at $\pi/2$ relative phase between the 1.5 μm quantum field and its LO, whereas the relative phase between the 0.8 μm quantum field and its LO was scanned. The observed squeezing and anti-squeezing levels were −6 dB and 16.4 dB, respectively.

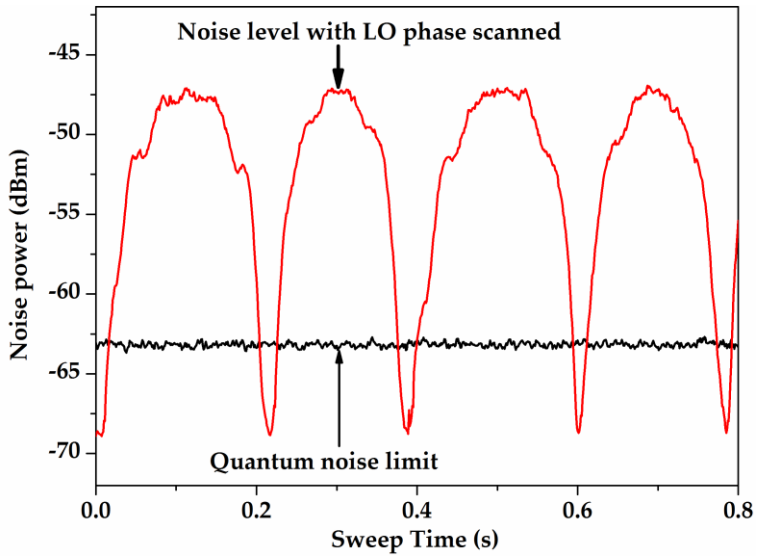

Figure 4. Quantum correlation noise of the phase quadrature sum. The measurement was recorded at an analysis frequency of 1 MHz, with a RBW (Resolution Band Width) of 200 kHz and a VBW (Video Band Width) of 100 Hz. The observed squeezing and anti-squeezing levels were −6 dB and 16.4 dB, respectively.

Figure 5 records the quantum correlation noise spectrum between the signal and idler beams at 1.5 μm and 0.8 μm in a broadband frequency range from 1 MHz to 5 MHz. The observed phase–quadrature sum and the amplitude–quadrature difference quantum correlation were −6 dB at 1 MHz, and −5 dB at 5 MHz. The decrease of the quantum correlation at an analysis frequency of 5 MHz was due to the finite linewidth (17 MHz) of the NOPA cavity.

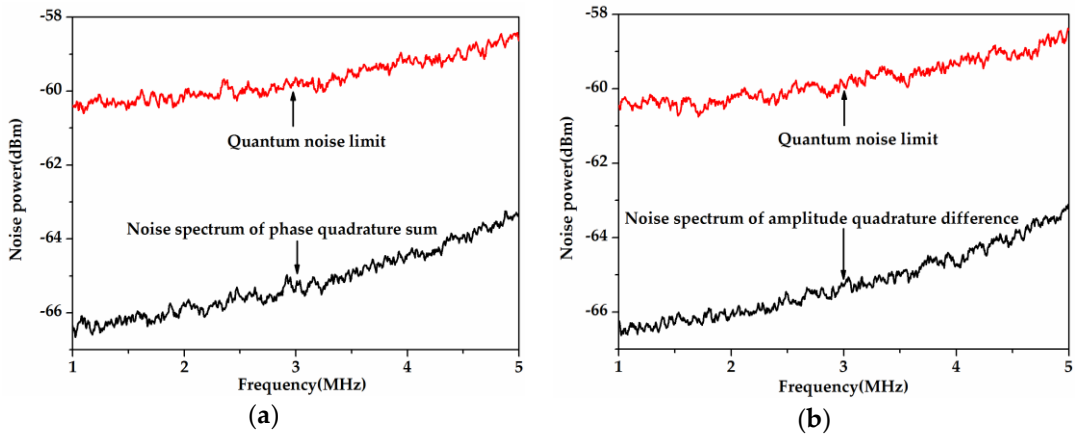

Figure 5. Measured broadband noise spectrum between the two-color down-converted optical fields from 1 MHz to 5 MHz. (**a**) phase quadrature sum; (**b**) amplitude quadrature difference. The RBW and VBW of the SA were 300 kHz and 100 Hz, respectively.

Table 1 lists the relevant parameters of both the former system and the current improved system. In the previous work, the measured quantum correlation of the amplitude quadrature difference, and the phase quadrature sum was ~3.3 dB, which subtracts the electronic dark noise; namely, η_{en} is 100%. For the current system, we improved the escape efficiency of the NOPA, the stability of the phase-locking servo system, and the detection efficiency. These approaches boosted the entanglement significantly from 3.3 dB to 6 dB.

Table 1. Comparison of experimental parameters between the two systems.

Works	T	L	η_{t}	η_{vis}	η_{pd}	η_{en}	θ (Mrad)	Observed Entangled Level (dB)
Guo et al. [6]	6.7%	1.6%	96%	94%	75%	100%	40	3.3
This work	10.2%	1.1%	96%	96%	92%	99.8%	8.7	6

Lacking appropriate single frequency laser sources at 0.8 microns and 1.5 microns, we could not determine the intracavity losses of the NOPA directly with a conventional method. Instead, we evaluate the intracavity losses based on the relationships between the measured amplitude quadrature difference (phase quadrature sum) quantum correlation, and the corresponding ideal quantum correlation at the pump level of $\frac{P}{P_{th}} = 0.6$. More precisely, we used the following beam splitter transformation equations, which modeled the effects of non-ideal efficiency:

$$\frac{\eta_{\mathrm{tot}}}{V_{Sq}^{0}} + 1 - \eta_{\mathrm{tot}} = V_{Anti-sq} \tag{6}$$

$$\eta_{\mathrm{tot}} V_{Sq}^{0} + 1 - \eta_{\mathrm{tot}} = V_{sq} \tag{7}$$

where V_{Sq}^{0} was the ideal quantum correlation assuming 100% efficiency, and V_{sq} and $V_{Anti-sq}$ were the measured quantum correlation and anti-correlation. Substituting the measured values of V_{sq} and $V_{Anti-sq}$ into Equations (6) and (7), the total efficiency η_{tot} and the ideal quantum correlation V_{Sq}^{0} of the system could be derived. Starting from the total efficiency η_{tot}, the intracavity loss L (both the linear loss and the nonlinear loss) could be easily derived. At this stage, by substituting the relevant parameters of $\eta_{\mathrm{tot}} = 0.763$, $\frac{P}{P_{th}} = 0.6$, and $\frac{f}{f_c} = 1/17$ into Equation (2), the theoretical entanglement level for the current improved system was calculated to be −5.97 dB, which is in good agreement with the observed value.

5. Conclusions

In summary, we have analyzed in detail the effects of various factors that affect the quantum entanglement for a NOPA system. Based on this, we designed a NOPA experimental system and prepared high-quality two-color CV quantum-entangled optical beams at 0.8 μm and 1.5 μm with 6.0 dB of entanglement. Since a high degree of entanglement is crucial for quantum information applications, the current system should be optimized further. For instance, we can enhance the transmission of the output coupler to 12%, the propagation efficiency to 99%, the interference efficiency to 99.8%, and the quantum efficiency of the photodiode to 99%. Then, the total loss will increase to 89.2%; in this situation, we can reach −8.9 dB of entanglement. If the intracavity loss is further reduced to 0.5%, a higher entanglement of −11 dB can be generated.

Acknowledgments: This work was supported by the Key Project of the National Key R&D Program of China (2016YFA0301403), the Natural National Science Foundation of China (NSFC) (11774209, 61378010), the Shanxi 1331KSC, and the Program for the Outstanding Innovative Teams of Higher Learning Institutions of Shanxi.

Author Contributions: Ning Wang and Shanna Du performed the experiments, Yongmin Li conceived the original research idea, Ning Wang and Yongmin Li developed the theoretical formalism, performed the data analysis, and wrote the manuscript.

Conflicts of Interest: The authors declare no conflict of interest.

References

1. Horodecki, R.; Horodecki, P.; Horodecki, M.; Horodecki, K. Quantum entanglement. *Rev. Mod. Phys.* **2009**, *81*, 865–942.
2. Ladd, T.D.; Jelezko, F.; Laflamme, R.; Nakamura, Y.; Monroe, C.; O'Brien, J.L. Quantum computers. *Nature* **2010**, *464*, 45.
3. Kimble, H.J. The quantum internet. *Nature* **2008**, *453*, 1023–1030.
4. Cerf, N.J.; Leuchs, G.; Polzik, E.S. *Quantum Information with Continuous Variables of Atoms and Light*; Imperial College Press: London, UK, 2007; p. 632.
5. Guo, X.M.; Xie, C.D.; Li, Y.M. Generation and homodyne detection of continuous-variable entangled optical beams with a large wavelength difference. *Phys. Rev. A* **2011**, *84*, 1892–1892.
6. Guo, X.M.; Zhao, J.J.; Li, Y.M. Robust generation of bright two-color entangled optical beams from a phase-insensitive optical parametric amplifier. *Appl. Phys. Lett.* **2012**, *100*, 091112.
7. Goda, K.; Miyakawa, O.; Mikhailov, E.E.; Saraf, S.; Adhikari, R.; Mchenzie, K.; Ward, R.; Vass, S.; Weinstein, A.J.; Mavalvala, N. A quantum-enhanced prototype gravitational-wave detector. *Nat. Phys.* **2008**, *4*, 472–476, doi:10.1038/nphys920.
8. Grote, H.; Danzmann, K.; Dooley, K.L.; Schnabel, R.; Slutsky, J.; Vahlbruch, H. First long-term application of squeezed states of light in a gravitational-wave observatory. *Phys. Rev. Lett.* **2013**, *110*, 181101.
9. Giovannetti, V.; Lloyd, S.; Maccone, L. Advances in quantum metrology. *Nat. Photonics* **2011**, *96*, 222–229.
10. Polzik, E.S.; Carri, J.; Kimble, H.J. Spectroscopy with squeezed light. *Phys. Rev. Lett.* **1992**, *68*, 3020.
11. Polzik, E.S.; Carri, J.; Kimble, H.J. Atomic spectroscopy with squeezed light for sensitivity beyond the vacuum-state limit. *Appl. Phys. B* **1992**, *55*, 279–290.
12. Li, Y.Q.; Lynam, P.; Xiao, M.; Edwards, P.J. Sub-shot-noise laser doppler anemometry with amplitude-squeezed light. *Phys. Rev. Lett.* **1997**, *78*, 3105–3108.
13. Li, Y.Q.; Guzun, D.; Xiao, M. Sub-shot-noise-limited optical heterodyne detection using an amplitude-squeezed local oscillator. *Phys. Rev. Lett.* **1999**, *82*, 5225–5228.
14. Madsen, L.S.; Usenko, V.C.; Lassen, M.; Filip, R.; Andersen, U.L. Continuous variable quantum key distribution with modulated entangled states. *Nat. Commun.* **2012**, *3*, 1083.
15. Ralph, T.C. Continuous variable quantum cryptography. *Phys. Rev. A* **1999**, *61*, 103031–103034.
16. Briegel, H.J.; Dür, W.; Cirac, J.I.; Zoller, P. Quantum repeaters for communication. *Phys. Rev. Lett.* **1998**, *81*, 5932.
17. Sangouard, N.; Simon, C.; Riedmatten, H.D.; Gisin, N. Quantum repeaters based on atomic ensembles and linear optics. *Rev. Mod. Phys.* **2009**, *83*, 33–34.
18. Azuma, K.; Tamaki, K.; Lo, H.K. All-photonic quantum repeaters. *Nat. Commun.* **2015**, *6*, 6787.
19. Schori, C.; Sorensen, J.L.; Polzik, E.S. Narrow-band frequency tunable light source of continuous quadrature entanglement. *Phys. Rev. A* **2002**, *66*, 355–358.
20. Villar, A.S.; Cruz, L.S.; Cassemiro, K.N.; Martinelli, M.; Nussenzveig, P. Generation of bright two-color continuous variable entanglement. *Phys. Rev. Lett.* **2005**, *95*, 243603.
21. Su, X.; Tan, A.; Jia, X.; Pan, Q.; Xie, C.; Peng, K. Experimental demonstration of quantum entanglement between frequency-nondegenerate optical twin beams. *Opt. Lett.* **2006**, *31*, 1133–1135.
22. Jing, J.; Feng, S.; Bloomer, R.; Pfister, O. Experimental continuous-variable entanglement of phase-locked bright optical beams. *Phys. Rev. A* **2006**, *4250*, 158–158.
23. Grosse, N.B.; Assad, S.; Mehmet, M.; Schnabel, R.; Symul, T.; Lam, P.K. Observation of entanglement between two light beams spanning an octave in optical frequency. *Phys. Rev. Lett.* **2008**, *100*, 243601.
24. Li, Y.; Guo, X.; Bai, Z.; Liu, C. Generation of two-color continuous variable quantum entanglement at 0.8 and 1.5 μm. *Appl. Phys. Lett.* **2010**, *97*, 093602–093601.
25. Liu, W.; Wang, N.; Li, Z.; Li, Y. Quantum frequency up-conversion of continuous variable entangled states. *Appl. Phys. Lett.* **2015**, *107*, 116.
26. Coelho, A.S.; Barbosa, F.A.S.; Cassemiro, K.N.; Villar, A.S.; Martinelli, M.; Nussenzveig, P. Three-color entanglement. *Science* **2009**, *326*, 823–826.
27. Yu, Y.; Ji, F.; Shi, Z.; Wang, H.J.; Zhao, J.; Wang, Y. Three-color entanglement generated by single-pass cascaded sum-frequency processes. *Laser Phys. Lett.* **2017**, *14*, 035202.
28. Jia, X.J.; Yan, Z.H.; Duan, Z.Y.; Su, X.; Wang, H.; Xie, C.D.; Peng, K.C. Experimental realization of three-color entanglement at optical fiber communication and atomic storage wavelengths. *Phys. Rev. Lett.* **2012**, *109*, 253604.

29. Zhang, Y.; Kasai, K.; Watanabe, M. Classical and quantum properties of optical parametric amplifier/deamplifier. *Phys. Lett. A* **2002**, *297*, 29–36.
30. Dwyer, S.; Barsotti, L.; Chua, S.S.Y.; Evans, M.; Factourovich, M.; Gustafson, D.; Isogai, T.; Kawabe, K.; Khalaidovski, A.; Lam, P.K.; et al. Squeezed quadrature fluctuations in a gravitational wave detector using squeezed light. *Opt. Express* **2013**, *21*, 19047–19060.
31. Breitenbach, G.; Schiller, S.; Mlynek, J. 81% conversion efficiency in frequency-stable continuous-wave parametric oscillation. *J. Opt. Soc. Am. B* **1995**, *12*, 2095–2101.
32. Fabre, C.; Rosencher, E. Oscillation characteristics of continuous-wave optical parametric oscillators: Beyond the mean-field approximation. *J. Opt. Soc. Am. B* **2002**, *19*, 1107–1116.
33. Coelho, A.S.; Cesar, J.E.S.; Cassemiro, K.N.; Villar, A.S.; Nussenzveig, P.; Martinelli, M. Extra phase noise from thermal fluctuations in nonlinear optical crystals. *Phys. Rev. A* **2009**, *79*, 063816.